


**Kinetics of contact processes under segregation**Tomás Aquino<sup>1,2,\*</sup> and Marco Dentz<sup>1</sup><sup>1</sup>Spanish National Research Council (IDAEA–CSIC), 08034 Barcelona, Spain<sup>2</sup>Geosciences Rennes, UMR 6118, CNRS, Université de Rennes 1, Rennes, France (Received 16 September 2019; revised manuscript received 14 November 2019; published 10 January 2020)

The kinetics of contact processes are determined by the interplay among local mass transfer mechanisms, spatial heterogeneity, and segregation. Determining the macroscopic behavior of a wide variety of phenomena across the disciplines requires linking reaction times to the statistical properties of spatially fluctuating quantities. We formulate the dynamics of advected agents interacting with segregated immobile components in terms of a chemical continuous-time random walk. The inter-reaction times result from the first-passage times of mobile species to and across reactive regions, and available immobile reactants undergo a restart procedure. Segregation leads to memory effects and enhances the role of concentration fluctuations in the large-scale dynamics.

DOI: [10.1103/PhysRevE.101.012114](https://doi.org/10.1103/PhysRevE.101.012114)**I. INTRODUCTION**

Mass-action reactions find applicability as population dynamics models of contact processes among agents, spanning biological processes [1], epidemiology [2], ecology [3], quantum molecular dynamics [4], and chemical reactions in geological media [5]. The large-scale dynamics of such processes are determined by the interplay among local mechanisms, spatial heterogeneity, and segregation. Transport limitations under segregation and spatial heterogeneity lead to inter-reaction times which are related to the first encounter time among reactants [6–10]. Broad reaction times result in mesoscopic dynamical coupling between transport and reaction due to memory effects [11,12]. In turn, the large-scale behavior may involve nonclassical, fluctuation-driven kinetics [13–15], broad reaction rate distributions [16], time-dependent reaction rates [17], and time-nonlocal kinetics [12]. The concept of residence time and its role in reactive transport have received much attention, in particular in hydrogeological applications [18,19]. This has led to the formulation of large-scale dynamics in terms of so-called stochastic-convective streamtube models, where reactive transport in the presence of physical and chemical heterogeneity is represented in terms of an ensemble of streamtubes [20–23].

The classical picture for stochastic reactions, corresponding to the Gillespie algorithm [24], assumes complete reactant mixing. It leads to exponential inter-reaction times and predicts the classical mass-action rate laws for large reactant numbers [25–27]. The recently proposed chemical continuous-time random walk (chCTRW) framework allows for more general inter-reaction times, leading to a broader class of large-scale rate laws, including time-nonlocal kinetics [28]. However, linking disorder properties, mass transfer, and inter-reaction times, a fundamental step toward the understanding and quantification of the emergence of large-scale

kinetics in the presence of spatial heterogeneity and reactant segregation, remains in general an open problem.

This work develops this link for advective transport under spatial chemical disorder. We consider segregated immobile reactants, which react with mobile components. Inter-reaction times relate directly to first-passage times (FPTs) of mobile reactants to and across reactive regions. On encountering a reactive region, mobile components come into contact with the locally available reactants. As we will see, this corresponds to a restart of the immobile reactants according to the original resident copy numbers. Processes under restart have received considerable attention in the context of chemical reactions and in particular as a framework for optimizing search strategies [29–32].

We derive a generalized master equation [33] for the chemical kinetics using the chCTRW framework, which we generalize to account for restart and parametrize in terms of the heterogeneity. The corresponding large-scale kinetics exhibit memory effects, and fluctuations about the average concentration play a role at large scales.

**II. MODEL**

We consider *mobile* reactants advected along separate trajectories. Advective velocity  $V$  is constant in each trajectory and independent and identically distributed according to a probability density function (PDF)  $\xi(\cdot)$  across trajectories. Additional reactants are confined to certain regions, see Fig. 1. We term these reactants *immobile* and these regions *reactive*. The latter are treated as well-mixed batch reactors, such that the chemical dynamics within proceed according to the classical Gillespie algorithm [24].

The length  $L_r$  of reactive regions is an independent and identically distributed random variable distributed according to the PDF  $\rho_r(\cdot)$ . The well-mixed assumption is difficult to justify if  $\rho_r$  has infinite moments. Instead, we assume  $L_r$  is characterized by a finite mean  $\ell_r$ , and for simplicity we set  $\rho_r(\ell) = e^{-\ell/\ell_r}/\ell_r$ . Segregation of immobile reactants is characterized by the PDF  $\rho_c(\cdot)$  of nonreactive region lengths

\*tomas.decamposaquino@univ-rennes1.fr.

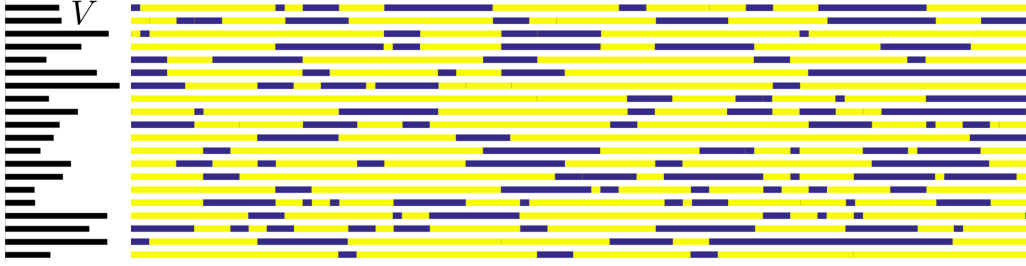


FIG. 1. Illustration of the model segregation structure. The velocity  $V$  of mobile species (proportional to black bar length) is constant along each separate trajectory and distributed across trajectories. Mass evolves according to reaction in reactive regions (blue), interspersed with nonreactive regions (yellow), both of distributed length.

$L_c$  between reactive regions, which are also independent and identically distributed. We distinguish the cases of *mild segregation*, corresponding to finite inter-reactive-region mean distance  $\ell_c$ , and *strong segregation*, corresponding to infinite mean distance,  $\rho_c(\ell) \approx (\ell/\ell_c)^{-1-\beta}/[\ell_c|\Gamma(-\beta)|]$  for  $\ell \gg \ell_c$ , where  $\Gamma(\cdot)$  is the gamma function,  $\ell_c$  is a characteristic length, and  $0 < \beta < 1$  [34]. We assume in what follows that mobile reactants begin within a reactive region to simplify the exposition. The general case of start in an arbitrary region, as illustrated in Fig. 1, can readily be treated in the framework developed below by including an additional waiting time until the first reaction, corresponding to the time to reach the first reactive region.

The idealized model set forth here retains the key features of segregation and will allow us to develop a quantitative model of its impact on chemical reactions. We consider in general a set of  $m_s$  species  $\mathcal{S}_j$ ,  $j = 1, \dots, m_s$ , which are subject to  $m_r$  reactions,  $\sum_{j=1}^{m_s} r_{ij}\mathcal{S}_j \rightarrow_{\kappa_i} \sum_{j=1}^{m_s} p_{ij}\mathcal{S}_j$ ,  $i = 1, \dots, m_r$ . Each reaction is characterized by its stoichiometry, with  $r_{ij}$  ( $p_{ij}$ ) denoting the number of reactants (products) of species  $j$  consumed (produced) by reaction  $i$ . Furthermore, each reaction is associated with an intrinsic (microscopic) reaction rate  $\kappa_i$  which fully determines its behavior under well-mixed conditions. All reactions involve immobile reactants, so that no reaction occurs outside reactive regions. The chemical state  $N(t)$  describes the number of mobile and immobile reactants of each species at time  $t$ . The net change in chemical state due to reaction  $i$  is described by the stoichiometry vectors  $s_i = \mathbf{p}_i - \mathbf{r}_i$ . Sub- or superscripts  $M, I$  denote quantities relating to mobile and immobile components, respectively. For example, the chemical state is decomposed into mobile and immobile components as  $N = (N_M, N_I)$  and the stoichiometry vectors as  $s_i = (s_i^M, s_i^I)$ . Throughout, we denote the Laplace transform by a tilde, the Laplace variable by  $\lambda$ , and ensemble averages (across trajectories) by angled brackets. A vertical bar is used to denote conditioning.

We introduce also some key quantities governing the dynamics. The mean time spent in a reactive region at velocity  $v$  is  $\mu(v) = \ell_r/v$ , so that  $1/\mu(v)$  is the probability per unit time for mobile reactants to exit a given reactive region and experience the delay induced by the subsequent nonreactive region. Reactive patches are associated with a Damköhler number  $\text{Da}(v) = \mu(v)a(\bar{n})/\bar{n}$ , where  $\bar{n}$  are characteristic copy numbers of each species (e.g., the initial state) and  $\bar{n}$  is an overall characteristic copy number (e.g., the average of  $\bar{n}$  across components or a component of interest). This

dimensionless number is the ratio of the characteristic transport and reaction times in a single reactive region. Finally, the ratio of characteristic nonreactive and reactive region lengths is denoted by  $\alpha = \ell_c/\ell_r$ .

### III. QUALITATIVE DYNAMICS OF REACTION UNDER SEGREGATION

In order to motivate the general theory developed below, we first illustrate the impact of segregation on the large-scale kinetics of the mobile-immobile degradation reaction  $\mathcal{S}_M + \mathcal{S}_I \rightarrow_{\kappa} \emptyset$ , where  $\mathcal{S}_M$  is mobile and  $\mathcal{S}_I$  is immobile. We consider both mild and strong segregation, specifically with exponential and Lévy-stable [34] inter-reactive region lengths. For simplicity, we set a fixed velocity  $V = v$  and a fixed number of initial immobile components  $n_{0,I}$  in each reactive region.

We consider an instantaneous, point initial injection of mobile components, and we simulate their average degradation under segregation for large particle numbers. When characteristic reactant numbers  $\bar{n} \rightarrow \infty$ , we may define continuous (number) concentrations  $C(t) = N(t)/\bar{n}$ . We take  $\bar{n}$  as the average initial number of reactants. The reaction in reactive patches then proceeds according to the well-mixed rate laws. For  $n_{M,I}$  mobile or immobile particles under well-mixed conditions, there are  $n_M n_I$  mobile-immobile particle pairs available for reaction. The reaction between each pair proceeds at the microscopic reaction rate  $\kappa$ . The reaction between *some* pair thus proceeds at a rate  $a(\mathbf{n}) = \kappa n_M n_I$ . In terms of concentrations, the well-mixed rate laws are thus given by

$$\frac{dc_{M,I}^{\text{wm}}(t)}{dt} = -\kappa^C c_M^{\text{wm}}(t) c_I^{\text{wm}}(t), \quad (1)$$

where  $\kappa^C = \bar{n}\kappa$  is a macroscopic reaction rate associated with well-mixed concentration decay. The analytical solution of this equation, along with details on the numerical simulations under segregation, is given in Appendix A.

The solid lines in Fig. 2 show the ensemble-averaged mobile concentrations  $\bar{c}_M(t)$ , normalized by the initial concentration  $c_{0,M}$ , as a function of time  $t$  for different values of Damköhler number  $\text{Da} = \kappa^C \mu c_{0,I}$ , where  $c_{0,I}$  is the initial immobile concentration in each reactive region. The evolution of concentration presents qualitative differences in the functional form of the decay with varying Damköhler

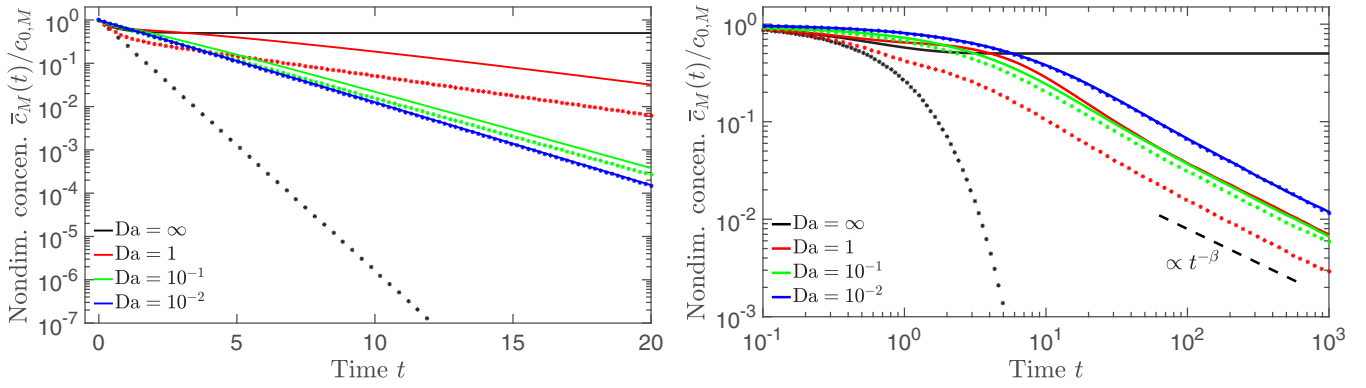


FIG. 2. Temporal evolution of concentration under the full degradation reaction  $\mathcal{S}_M + \mathcal{S}_I \rightarrow \emptyset$  (solid lines) and the catalytic degradation reaction  $\mathcal{S}_M + \mathcal{S}_I \rightarrow_{\kappa} \mathcal{S}_I$  (markers) for different values of Damköhler number  $Da$ . The initial conditions for mobile and immobile concentrations are  $c_{0,M} = 4/3$  and  $c_{0,I} = 2/3$ . Fixed parameters are  $\alpha = 2$ ,  $v = 4$ , and  $\kappa^C = 2$ , and  $Da$  is set by varying  $\ell_r$ . Concentrations are averaged over  $10^5$  realizations. Left: Mild segregation, with exponentially distributed nonreactive region lengths. Right: Strong segregation, with Lévy-stable-distributed nonreactive region lengths with exponent  $\beta = 0.7$ .

number. For mild segregation (left panel), the decay at low  $Da$  is always exponential, but slower-than-exponential decay is present for longer times as  $Da$  increases. Under strong segregation (right panel), we observe power-law decay for all finite  $Da$ , characterized by the exponent  $\beta$  associated with the inter-reactive-region lengths. The solutions for a single well-mixed patch, corresponding to the  $Da \rightarrow \infty$  limit, are also shown. In this case, the concentration initially decays faster than in the segregated systems. However, due to depletion of the initial immobile concentration, which in this example is lower than the initial mobile concentration, reaction then slows down and the mobile concentration approaches equilibrium.

The impact of segregation on reaction dynamics, illustrated here for this simple degradation reaction, is in general due to two factors. First, reaction is punctuated by times spent in nonreactive regions, which leads to an effective reaction slowdown. Second, mobile components react only with the locally available immobile reactants in a given region. When a reactive region is left and a subsequent one is entered, there is a restart of available immobile reactants, according to their initially available concentration. In order to highlight the role of immobile reactant depletion and restart, the markers in Fig. 2 show the evolution of mobile concentrations for the catalytic degradation reaction  $\mathcal{S}_M + \mathcal{S}_I \rightarrow_{\kappa} \mathcal{S}_I$ , using the same parameter values as before. In this case, the immobile component acts as a catalyst, and it is thus neither consumed nor subject to the effect of restart. For a single well-mixed patch, in the  $Da \rightarrow \infty$  limit, the mobile species' decay is then purely exponential and always faster than under segregation. However, as  $Da \rightarrow 0$ , corresponding to negligible reaction within each single region, the decay of mobile concentration becomes identical under the two reactions.

#### IV. THEORY

In what follows, we will discuss and quantify the mechanisms discussed in the previous section. To this end, we develop a general framework for arbitrary reaction dynamics under spatial segregation.

#### A. Catalytic reactions

We start by examining the case where the immobile components serve as catalysts, i.e., they participate in the reactions but are not consumed or produced ( $s_i^t = 0$ ). We further assume for the moment that the immobile reactants are present in identical copy numbers in each reactive region. In this case, the dynamics proceed identically with the classical well-mixed scenario, except the periods of availability of reactants are punctuated by waiting times due to segregation. We proceed to find the chCTRW description of this system in terms of a generalized master equation, starting from the determination of the inter-reaction times.

##### 1. Inter-reaction times

The lack of memory of the exponential distribution implies that the distribution of distances to the end of reactive regions, starting from any point within a reactive region, has the same length distribution as the full regions [27]. Thus, it is sufficient to study inter-reaction times starting at the beginning of reactive regions.

Consider a given chemical state  $N(t) = \mathbf{n}$  and velocity  $V = v$ . For advective transport, the FPT across reactive and conservative regions is given by the crossing time  $L_{r,c}/v$ . Thus, the corresponding PDFs are given by  $\psi_{r,c}(t|v) = v\rho_{r,c}(vt)$ . Following chCTRW theory, we write the inter-reaction times as  $\tau(\mathbf{n}, v) = \tau_r(\mathbf{n}) + \tau_c(\tau_r, v)$ . The intrinsic reaction time  $\tau_r$  represents reaction in the absence of segregation. It depends on the current chemical state and corresponds to time spent in reactive regions, where reaction proceeds according to the classical well-mixed theory. Let  $\phi_i^r(t|\mathbf{n}) dt$  represent the joint probability that, in the absence of segregation, reaction  $1 \leq i \leq m_r$  fires next and after a waiting time in  $[t, t + dt]$ . Then,  $\tau_r(\mathbf{n})$  has PDF  $\phi^r(t|\mathbf{n}) = \sum_i \phi_i^r(t|\mathbf{n})$  (see Appendix B for a brief overview of the well-mixed description). The additional global delay  $\tau_c$  is caused by segregation. It corresponds to time spent in nonreactive regions, which is fully determined by the current  $\tau_r$  and does not depend further on the chemical state. Specifically, a given time  $\tau_r = t_r$  corresponds to fully traversing a certain number  $\eta(t_r, v)$  of reactive regions,

and  $\tau_c(t_r, v) = \sum_{k=1}^{\eta(t_r, v)} L_{c,k}/v$ , where the  $L_{c,k}$  are independent and identically distributed according to  $\rho_c$ . For exponential reactive lengths,  $\eta(t_r, v)$  is Poisson-distributed, as shown in Appendix C. Thus, segregation leads to a compound-Poisson inter-reaction delay. According to Ref. [28], the full inter-reaction time density is then related to the intrinsic inter-reaction time density by

$$\tilde{\phi}_i(\lambda|\mathbf{n}, v) = \tilde{\phi}_i^r[\lambda/\tilde{K}(\lambda|v)|\mathbf{n}, v], \quad (2)$$

where

$$\tilde{K}(\lambda|v) = \left[ 1 + \frac{1 - \tilde{\psi}_c(\lambda|v)}{\mu(v)\lambda} \right]^{-1} \quad (3)$$

is the Laplace transform of a memory kernel, as we will see shortly.

## 2. Generalized master equation

We first define the probabilities  $\gamma_i(\mathbf{n}|\mathbf{n}')$  of reaction  $i$  yielding the chemical state  $\mathbf{n}$ , given the starting state  $\mathbf{n}'$ . The change in state is given by the stoichiometry vector  $s_i$ . Thus,

$$\gamma_i(\mathbf{n}|\mathbf{n}') = \delta_{\mathbf{n}, \mathbf{n}'+s_i}, \quad (4)$$

where  $\delta_{\cdot, \cdot}$  is the Kronecker delta. According to the general theory developed in Ref. [28], the generalized master equation for the ensemble-averaged propagator of the chemical state, given initial state  $\mathbf{n}_0$  and velocity  $v$ , is then given by

$$\begin{aligned} \frac{\partial p(\mathbf{n}, t|\mathbf{n}_0, v)}{\partial t} &= \sum_{\mathbf{n}' \geq 0} \sum_{i=1}^{m_r} \int_0^t dt' [\gamma_i(\mathbf{n}|\mathbf{n}') - \delta_{\mathbf{n}, \mathbf{n}'}] \\ &\times M_i(t - t'|\mathbf{n}', v) p(\mathbf{n}', t'|\mathbf{n}_0, v), \end{aligned} \quad (5)$$

where the Laplace transforms of the memory functions are given in terms of the inter-reaction time densities as

$$\tilde{M}_i(\lambda|\mathbf{n}, v) = \frac{\lambda \tilde{\phi}_i(\lambda|\mathbf{n}, v)}{1 - \sum_{i=1}^{m_r} \tilde{\phi}_i(\lambda|\mathbf{n}, v)}. \quad (6)$$

Using Eq. (13) together with the well-mixed description, we obtain

$$\tilde{M}_i(\lambda|\mathbf{n}, v) = \tilde{K}(\lambda|v) a_i(\mathbf{n}), \quad (7)$$

with  $a_i(\mathbf{n}) = \kappa_i h_i(\mathbf{n})$  and  $a(\mathbf{n}) = \sum_{i=1}^{m_r} a_i(\mathbf{n})$ , where the  $\kappa_i$  are microscopic rate constants and the  $h_i(\mathbf{n})$  encode the dependency of the rates on the state. In the absence of segregation,  $\psi_c(t) = \delta(t)$ . Equation (3) with  $\tilde{\psi}_c(\lambda) = 1$  leads to  $\tilde{K}(\lambda|v) = 1$ , and therefore  $K(t|v) = \delta(t)$ . This recovers the classical chemical master equation [25]. We thus see that  $K$  plays the role of a memory kernel describing reaction slowdown due to segregation. Reactions under compound-Poisson delay, and corresponding simulation techniques to solve the generalized master equation (5), are discussed in general terms in Ref. [28]. Note that for catalytic reactions,  $s_i^I = 0$  implies immobile copy numbers do not change, and it is sufficient to consider the evolution of the mobile components.

As an example, consider the catalytic degradation reaction introduced in Sec. III. We have  $h_1(\mathbf{n}) = n_M n_I$ , the number of pairs of mobile-immobile particles, and  $a(\mathbf{n}) = a_1(\mathbf{n}) = \kappa n_M n_I$ . The intrinsic waiting time density is given by  $\phi_1^r(t|\mathbf{n}) = a(\mathbf{n}) \exp[a(\mathbf{n})t]$ , and the single memory function is

$\tilde{M}_1(\lambda|\mathbf{n}, v) = \tilde{K}(\lambda|v) a(\mathbf{n})$ . The stoichiometry vector is  $s_1 = (-1, 0)$ . Thus, the master equation for the mobile components becomes

$$\begin{aligned} \frac{\partial p(n_M, t)}{\partial t} &= - \int_0^t dt' K(t-t') [a(n_M, n_{0,I}) p(n_M, t') \\ &\quad - a(n_M + 1, n_{0,I}) p(n_M + 1, t')], \end{aligned} \quad (8)$$

where we have omitted the dependency on the initial condition and  $v$  for notational brevity.

The ensemble-averaged probability of a given state at a given time is in general obtained by averaging over velocities and initial conditions. Denote by  $\gamma_M(\cdot|v)$  the initial distribution of mobile components at injection and by  $\gamma_I(\cdot|v)$  the initial distribution of immobile reactant numbers across reactive regions, given velocity  $v$ . The initial copy number distribution at the first reactive region is thus  $\gamma(\mathbf{n}|v) = \gamma_M(\mathbf{n}_M|v) \gamma_I(\mathbf{n}_I|v)$ . For equal initial immobile component copy numbers  $n_{0,I}$  in each reactive patch,  $\gamma_I(\mathbf{n}|v) = \delta_{\mathbf{n}, n_{0,I}}$ . The probability of finding the state  $N(t) = \mathbf{n}$  at time  $t$  is  $p(\mathbf{n}, t) = \langle p[\mathbf{n}, t|N_0(V), V] \rangle$ , where for each  $V = v$  the initial condition  $N_0(v)$  is distributed according to  $\gamma(\cdot|v)$ . We note also that the propagator contains all necessary information to compute spatial quantities. Spatial distributions may be obtained by multiplying the propagator by the probability that mobile reactants are at position  $x$  at time  $t$  before averaging, which, assuming mobile species start at  $x = 0$  at  $t = 0$ , is given here by the Dirac delta  $\delta(x - Vt)$ . Similarly, concentrations fluxes at a control plane at distance  $x$  as a function of time  $t$  are obtained by multiplying by the FPT to distance  $x$ , given here by  $\delta(t - x/V)$ .

## B. General reactions

We now study the general case where reactions may involve net production or consumption of immobile components and where different reactive regions may initially comprise different copy numbers of immobile reactants. In this case, as the mobile reactants reach each reactive region, they encounter the initial resident copy numbers. These are then depleted or produced according to reaction. Once the mobile components exit a given reactive region and arrive at the subsequent one, they again encounter resident copy numbers according to their initial distribution. This leads naturally to the concept of restart of immobile components. Developing a generalized master equation for these dynamics thus requires generalizing the inter-reaction times to account for restart.

### 1. Inter-reaction times under restart

In order to make use of the techniques developed in Ref. [28], we require that the dynamics be a Markov process in reaction step. For exponential reactive region lengths, whenever a reaction fires, the leftover reactive region length is identically distributed with the full region length, as discussed above. However, if the initial number of immobile reactants depends on the reactive region length, then the number of immobile reactants then gives information about the region length, and the inter-reaction times are no longer independent of past history. We assume here that this is not the case.

Consider a given chemical state  $N(t) = \mathbf{n}$ , velocity  $V = v$ , and lengths of a consecutive reactive-nonreactive region pair  $L_{r,c}$ . The effect of restart may be treated as a special reaction, which we number  $i = 0$ . It fires after a time  $L_r/v$  and leads to restart of the immobile components after a time  $(L_r + L_c)/v$ . The next reaction to fire is the one with the minimum inter-reaction time, including restart. The inter-reaction time densities, given the chemical state, velocity, and region lengths, are defined such that  $\phi_i(t|\mathbf{n}, v, L_r, L_c) dt$  is the joint probability of reaction  $i$  firing and the inter-reaction time being in  $[t, t + dt]$ . Under restart, we write

$$\phi_i(t|\mathbf{n}, v, L_r, L_c) = b_i(\mathbf{n}, v, L_r)\phi_i(t|\mathbf{n}, v, L_r, L_c), \quad (9)$$

where  $b_i(\mathbf{n}, v, L_r)$  is the propensity of reaction  $i$ , i.e., the probability that it fires next, and  $\phi_i(\cdot|\mathbf{n}, v, L_r, L_c)$  is the inter-reaction time PDF of reaction  $i$  given that it will fire next. Restart occurs if the minimum reaction time is larger than the restart time  $L_r/v$ . This happens with probability  $\int_{L_r/v}^{\infty} dt \phi^r(t|\mathbf{n}) = \exp[-a(\mathbf{n})L_r/v]$ . Otherwise, with probability  $1 - \exp[-a(\mathbf{n})L_r/v]$ , the normal reaction with the minimum inter-reaction time fires. Thus,

$$b_i(\mathbf{n}, v, L_r) = \begin{cases} e^{-a(\mathbf{n})L_r/v} \\ [1 - e^{-a(\mathbf{n})L_r/v}] \frac{a_i(\mathbf{n})}{a(\mathbf{n})} \end{cases}. \quad (10)$$

Here and in what follows, the first case refers to  $i = 0$  (restart) and the second to  $1 \leq i \leq m_r$  (regular reactions). The inter-reaction time PDFs must also be conditioned on  $t < L_r/v$  for the regular reactions, and the waiting time associated with restart is  $(L_r + L_c)/v$ , so that

$$\phi_i(t|\mathbf{n}, v, L_r, L_c) = \begin{cases} \delta(t - \frac{L_r+L_c}{v}) \\ \frac{a(\mathbf{n}) \exp[-a(\mathbf{n})t]}{1 - \exp[-a(\mathbf{n})L_r/v]} H(\frac{L_r}{v} - t) \end{cases}, \quad (11)$$

where  $H$  is the Heaviside step function. Thus, according to Eq. (9),

$$\phi_i(t|\mathbf{n}, v, L_r, L_c) = \begin{cases} e^{-a(\mathbf{n})L_r/v} \delta(t - \frac{L_r+L_c}{v}) \\ a_i(\mathbf{n}) e^{-a(\mathbf{n})t} H(\frac{L_r}{v} - t) \end{cases}. \quad (12)$$

Defining  $\phi_i(t|\mathbf{n}, v) = \langle \phi_i(t|\mathbf{n}, v, L_r, L_c) \rangle$ , we find the Laplace transforms

$$\tilde{\phi}_i(\lambda|\mathbf{n}, v) = \begin{cases} \tilde{\psi}_r[\lambda + a(\mathbf{n})|v] \tilde{\psi}_c(\lambda|v) \\ a_i(\mathbf{n}) \frac{1 - \tilde{\psi}_r[\lambda + a(\mathbf{n})|v]}{\lambda + a(\mathbf{n})} \end{cases}. \quad (13)$$

The inter-reaction times are thus fully determined by first-passage properties together with the rates  $a_i(\mathbf{n})$ .

## 2. Generalized chemical master equation under restart

We turn to the generalized master equation incorporating the effect of restart. The transition probabilities  $\gamma_i(\mathbf{n}|\mathbf{n}')$  corresponding to the regular reactions remain given by Eq. (4), as the effect of these reactions does not change. The effect of the restart reaction, conditioned on a given velocity  $v$ , is characterized by:

$$\gamma_0(\mathbf{n}|\mathbf{n}', v) = \gamma_I(\mathbf{n}_I|v) \delta_{\mathbf{n}_M, \mathbf{n}'_M}, \quad (14)$$

meaning that mobile reactants remain unaffected, and immobile copy numbers are redrawn from the initial distribution

as discussed above. As shown in detail in Appendix D, the generalized master equation corresponding to the dynamics under restart retains the same form as Eq. (5), with the memory functions again given in terms of the inter-reaction time densities according to Eq. (6). However, sums over reactions in both these equations now extend to  $i = 0$ , the reaction describing restart, and the inter-reaction time densities are given by Eq. (13). Direct computation shows that the modified inter-reaction times lead to the same memory functions for the regular reactions, as given by Eq. (7). Restart is associated with the memory function

$$M_0(\mathbf{n}|\mathbf{n}', v) = \tilde{K}(\lambda|v) \tilde{\psi}_c(\lambda)/\mu(v). \quad (15)$$

These results follow from the fact that normal reactions proceed at rate  $a_i(\mathbf{n})$  in reactive regions, whereas restart occurs at rate  $1/\mu(v)$  and is associated with an additional delay corresponding to traversing a nonreactive region. Realizations of these dynamics may be simulated with recourse to a generalized Gillespie algorithm under restart, which we outline in Appendix E.

Consider as an example the full degradation of Sec. III, with equal initial copy numbers of immobile components  $n_{0,I}$  in each reactive region. The stoichiometry vector is  $\mathbf{s}_1 = (-1, -1)$  and  $\gamma_0 = \delta_{n_I, n_{0,I}} \delta_{n_M, n'_M}$ . Similarly to Eq. (8) for the catalytic degradation example, we find the master equation

$$\begin{aligned} \frac{\partial p(n_M, n_I, t)}{\partial t} = & - \int_0^t dt' K(t-t') [a(n_M, n_I) p(n_M, n_I, t') \\ & - a(n_M + 1, n_I + 1) p(n_M + 1, n_I + 1, t')] \\ & - \int_0^t dt' K_c(t-t') [a(n_M, n_I) p(n_M, n_I, t') \\ & - a(n_M, n_{0,I}) p(n_M, n_{0,I}, t')], \end{aligned} \quad (16)$$

where the memory kernel associated with restart is given by the convolution  $K_c(t) = \int_0^t dt' K(t-t') \rho_c(t')$ , and we have again omitted dependencies on the initial condition and  $v$ .

## C. Restart and catalytic reactions

Consider equal initial immobile copy numbers in all reactive regions as in Sec. IV A. Since for catalytic reactions  $\mathbf{s}_i^I = 0$ , immobile copy numbers do not change due to either restart or regular reactions, the  $i = 0$  term in the master equation is null, and we recover catalytic dynamics, Eq. (5).

The catalytic description also plays a role as the limiting behavior for slow reaction. For small Damköhler number,  $\text{Da} \ll 1$ , the dynamics are transport dominated at the scale of a single region, meaning that many reactive regions must be visited before appreciable change due to reaction can occur. For fixed initial immobile copy numbers, the reset mechanism ensures there is no appreciable change in immobile copy numbers. The catalytic description is then valid for arbitrary reactions, and the subordination formulation of Ref. [28] holds. Note also that under these conditions, for arbitrary initial copy numbers, the dynamics are independent of the specific reactive region length distribution as long as it has a finite mean, see Appendix C.

### D. Large-scale kinetics

Next, we obtain the large-scale description corresponding to the mesoscopic master equations developed in the previous sections. In the large-particle-number limit, we work in terms of concentrations  $\mathbf{C}(t) = N(t)/\bar{n}$  as introduced in Sec. III. Correspondingly, we define  $a_i^C(\mathbf{c}) = \kappa_i^C h_i^C(\mathbf{c})$ ,  $a^C(\mathbf{c}) = \sum_{i=1}^{m_r} a_i^C(\mathbf{c})$ , with  $\kappa_i^C = \bar{n}^{\sum_{j=1}^{m_s} r_{ij} - 1} \kappa_i / \prod_{j=1}^{m_s} r_{ij}!$  as the macroscopic rate constants and  $h_i^C(\mathbf{c}) = \prod_{j=1}^{m_s} c_j^{r_{ij}}$ . Note that these quantities are fully defined in terms of their microscopic equivalents. For example, considering again the degradation reaction of Sec. III, we have  $\kappa^C = \bar{n}\kappa$  and  $h_1^C(\mathbf{n}) = c_M c_I$ , from which  $a^C(\mathbf{c}) = a_1^C(\mathbf{c}) = \kappa^C c_A c_B$ , the usual rate in the well-mixed rate laws for concentration. The average initial numbers of immobile components for velocity  $v$  are denoted by  $\bar{c}_{0,I}(v)$  and the average concentrations for initial condition  $\mathbf{c}_0$  and velocity  $v$  by  $\bar{\mathbf{c}}(t|\mathbf{c}_0, v) = \langle \mathbf{C}(t) | \mathbf{c}_0, v \rangle$ .

#### 1. Dynamical equations

In Appendix F, we show that the ensemble-averaged concentrations obey the integro-differential dynamical equations

$$\begin{aligned} \frac{d\bar{\mathbf{c}}_M(t|\mathbf{c}_0, v)}{dt} &= \int_0^t dt' K(t-t'|v) \sum_{i=1}^{m_r} s_i^M \langle a_i^C[\mathbf{C}(t')] | \mathbf{c}_0, v \rangle, \\ \frac{d\bar{\mathbf{c}}_I(t|\mathbf{c}_0, v)}{dt} &= \sum_{i=1}^{m_r} s_i^I \langle a_i^C[\mathbf{C}(t)] | \mathbf{c}_0, v \rangle \\ &\quad - \mu(v)^{-1} [\bar{\mathbf{c}}_I(t|\mathbf{c}_0, v) - \bar{\mathbf{c}}_{0,I}(v)]. \end{aligned} \quad (17)$$

Segregation induces memory effects in the form of a convolution with a memory kernel for the mobile components. For the immobile components, restart leads to a mean-reverting forcing term. For mild segregation, the memory is short term, and the late-time rate equations are time local, whereas memory is long range under strong segregation and the late-time rate equations involve nonlocal fractional derivatives [35].

In the classical rate laws, fluctuations vanish in the large-particle-number limit and  $\langle a_i^C[\mathbf{C}(t)] | \mathbf{c}_0, v \rangle = a_i^C[\bar{\mathbf{c}}(t|\mathbf{c}_0, v)]$  [27]. Here this is not the case. Under strong segregation, realizations of the dynamics break ergodicity weakly due to large fluctuations in the inter-reaction times, leading to persistent fluctuations about the average concentrations [28]. Under mild segregation, short-term memory effects coupled with the discontinuous changes in immobile concentrations caused by restart also prevent the fluctuations from vanishing. While equations for higher moments of the concentration can be found by appropriate averaging of the generalized master equation (5), these depend on still higher moments, and closed rate equations for the average components do not exist in general. In other words, fluctuations play an important role in the mean behavior, analogously to Ovchinnikov-Zeldovich segregation in a bimolecular annihilation reaction between diffusing components [13,36]. A common approach is to employ moment closure approximations [37,38], a technique that must be adapted to specific reactions and which we do not explore here. We employ stochastic algorithms, outlined in Appendix E, to numerically solve for the exact average concentration. We note here that the mean-reverting term

in the large-scale description of immobile concentration depends only on average concentrations. Thus, the catalytic description (for catalytic reactions or the low-Damköhler limit of general reactions, see Secs. IV A and IV C) holds at the large scale even if initial immobile copy numbers vary across reactive regions.

#### 2. Asymptotics

We now examine the asymptotic behavior of the large-scale kinetics. For mild segregation, under which the inter-reactive-region lengths have a mean, the Laplace transform of the corresponding FPT is approximated by  $\tilde{\psi}_c(\lambda|v) \approx 1 - \alpha\mu(v)\lambda$  for  $\lambda \ll 1/[\alpha\mu(v)]$ , corresponding to large times compared to the mean time to traverse a nonreactive region. To leading order in  $\lambda \ll 1/[(1+\alpha)\mu(v)]$  (corresponding to large times compared to the mean time to traverse a reactive and a nonreactive region),

$$\tilde{M}_i(\lambda|\mathbf{n}, v) = \frac{1}{1+\alpha} \left\{ \frac{1/\mu(v)}{a_i(\mathbf{n})} \right\}. \quad (18)$$

This leads to time-local equations for the mobile components at late times,

$$\frac{d\bar{\mathbf{c}}_M(t|\mathbf{c}_0, v)}{dt} = (1+\alpha)\mu(v)^2 \sum_{i=1}^{m_r} s_i^M \langle a_i^C[\mathbf{C}(t)] | \mathbf{c}_0, v \rangle. \quad (19)$$

For strong segregation, under which the inter-reactive region lengths do not have a mean, we have instead the small- $\lambda$  expansion  $\tilde{\psi}_c(\lambda|v) \approx 1 - [\alpha\mu(v)\lambda]^\beta$ ,  $0 < \beta < 1$ . To leading order in  $\lambda \ll 1/[(1+\alpha)\mu(v)]$ ,

$$\tilde{M}_i(\lambda|\mathbf{n}, v) = \mu(v)\lambda[\alpha\mu(v)\lambda]^{-\beta} \left\{ \frac{1/\mu(v)}{a_i(\mathbf{n})} \right\}, \quad (20)$$

yielding, at late times, the time-nonlocal equations

$$\frac{d^\beta \bar{\mathbf{c}}_M(t|\mathbf{c}_0, v)}{dt^\beta} = [\alpha\mu(v)]^\beta \mu(v) \sum_{i=1}^{m_r} s_i^M \langle a_i^C[\mathbf{C}(t)] | \mathbf{c}_0, v \rangle, \quad (21)$$

where  $d^\beta/dt^\beta$  denotes the Riemann-Liouville fractional derivative of order  $\beta$  [35].

### V. LARGE-SCALE DYNAMICS OF REACTION UNDER SEGREGATION

In order to illustrate the main features of the theoretical developments in the context of a particular reaction, let us return to the large-scale dynamics of mobile concentration for the degradation reaction  $S_M + S_I \rightarrow_\kappa \emptyset$  introduced in Sec. III. As the Damköhler number  $\text{Da}(v) = \kappa^C \mu(v) \bar{c}_{0,I}(v) \rightarrow 0$ , the changes in immobile concentration due to reaction in each region become arbitrarily small, so that  $\langle C_I C_M \rangle \approx \bar{c}_{0,I}(v) \langle C_M \rangle$  at all times. Thus, for small  $\text{Da}$ , the late-time rate equation for the mobile component under mild segregation is, according to Eq. (19),

$$\frac{d\bar{\mathbf{c}}_M(t|\mathbf{c}_0, v)}{dt} = - \frac{\text{Da}(v)}{(1+\alpha)\mu(v)} \bar{\mathbf{c}}_M(t|\mathbf{c}_0, v). \quad (22)$$

There is no appreciable reaction before the late-time equation is valid, so that the initial condition  $\mathbf{c}_{0,M}$  may be employed,

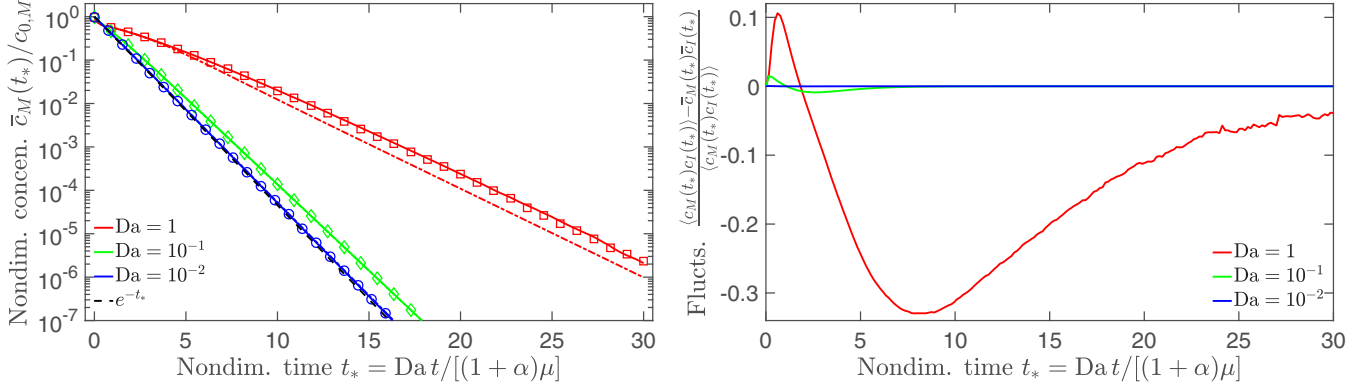


FIG. 3. Temporal evolution of concentration for  $\mathcal{S}_M + \mathcal{S}_I \rightarrow_{\kappa} \emptyset$  under mild segregation for different values of Damköhler number  $Da$ . Symbols represent stochastic simulations based on the Gillespie algorithm ( $10^7$  initial mobile particles and  $5 \times 10^6$  immobile particles per reactive region, averaged over  $10^5$  realizations) and solid lines employ the well-mixed rate equations in reactive regions ( $10^6$  realizations). Nonreactive region lengths are exponentially distributed. Fixed parameters are  $\alpha = 2$ ,  $v = 4$ , and  $\kappa^C = 2$ , and  $Da$  is set by varying  $\ell_r$ . Dash-dotted lines (overlapping the solid lines for low  $Da$ ) are numerical solutions of Eq. (17) using  $\langle C_M C_I \rangle = \bar{c}_M \bar{c}_I$ . Left: Average mobile concentration. The dashed line is the analytical solution in the limit of small Damköhler. Right: Concentration fluctuations.

and

$$\bar{c}_M(t|c_0, v) = c_{0,M} \exp \left[ -\frac{Da(v)t}{(1 + \alpha)\mu(v)} \right]. \quad (23)$$

Under strong segregation, the Laplace transform of the late-time equation (21) is, for  $Da(v) \ll 1$ ,

$$\frac{[\alpha\mu(v)\lambda]^\beta}{Da(v)} [\tilde{c}_M(t|c_0, v) - \lambda^{-1}c_{0,M}] = -\tilde{c}_M(\lambda|c_0, v). \quad (24)$$

Noticing that, for small  $\lambda$ , the initial-condition term on the left-hand side dominates, and inverting the Laplace transform,

$$\bar{c}_M(t|c_0, v) \approx \frac{c_{0,M}}{Da(v)\Gamma(1 - \beta)} \left[ \frac{t}{\alpha\mu(v)} \right]^{-\beta}. \quad (25)$$

Simulation results for mild segregation are shown in Fig. 3 and for strong segregation in Fig. 4. We consider for concreteness exponential  $\rho_c$  for mild and Lévy-stable  $\rho_c$  for strong segregation, as before. Note that, unlike in Fig. 2, time is

nondimensionalized so as to highlight the collapse of the low-Damköhler behavior onto the  $Da$ -independent curve valid for both the full degradation reaction and the catalytic degradation reaction  $\mathcal{S}_M + \mathcal{S}_I \rightarrow_{\kappa} \mathcal{S}_I$ . Under this nondimensionalization, higher  $Da$  leads to slower decay due to the effect of depletion of the immobile component. We compare a full stochastic algorithm employing the Gillespie method in reactive regions to a more efficient algorithm, valid for large particle numbers, which makes use of the well-mixed rate equations as in Sec. III (see Appendix E). The results are in very good agreement.

For mild segregation, simulations suggest that  $\langle C_I C_M \rangle \approx \bar{c}_{0,I}(v)\langle C_M \rangle$  holds at late times, as expected under finite-mean inter-reaction times (see the right panel of Fig. 3). Thus, the late-time concentration for each velocity  $v$  decays in general exponentially as argued above, but the leading coefficient differs because the appropriate initial condition for the late-time equation depends on the dynamics before it becomes valid.

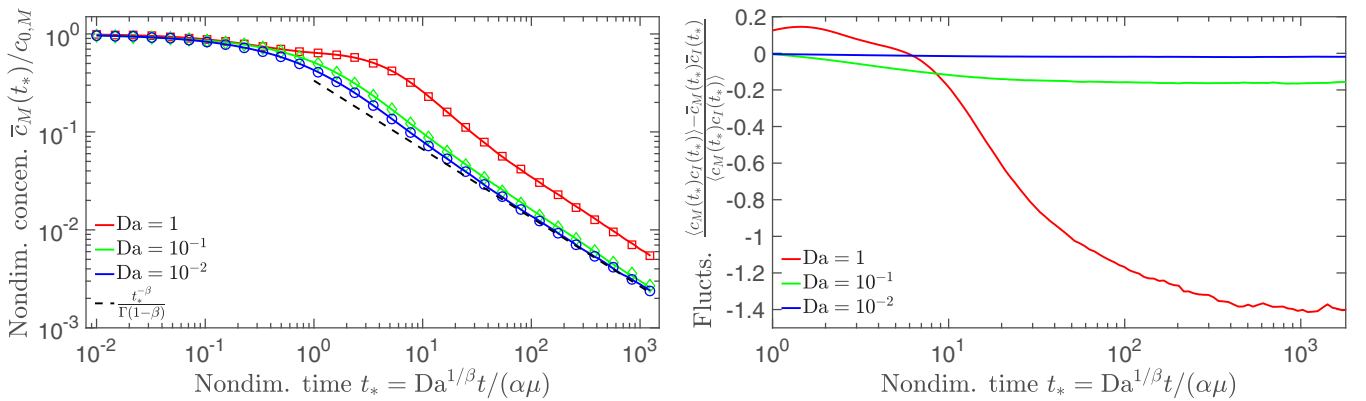


FIG. 4. Temporal evolution of concentration for  $\mathcal{S}_M + \mathcal{S}_I \rightarrow_{\kappa} \emptyset$  under strong segregation for different values of Damköhler number  $Da$ . Symbols represent stochastic simulations based on the Gillespie algorithm ( $10^7$  initial mobile particles and  $5 \times 10^6$  immobile particles per reactive region) and solid lines employ the well-mixed rate equations in reactive regions. All results are averaged over  $10^5$  realizations. Nonreactive region lengths are Lévy-stable-distributed with exponent  $\beta = 0.7$ . Fixed parameters are  $\alpha = 2$ ,  $v = 4$ , and  $\kappa^C = 2$ , and  $Da$  is set by varying  $\ell_r$ . Left: Average mobile concentration. The dashed line is the late-time analytical solution in the limit of small Damköhler. Right: Concentration fluctuations.

However, for large  $Da$ , the exponential asymptotic regime is not observed, as the concentration reaches very small values before it occurs. We show also the solution obtained by numerically integrating the closed rate equations obtained by setting  $\langle C_M C_I \rangle = \bar{c}_M \bar{c}_I$  in Eq. (17) (see Appendix F). Its breakdown for  $Da \gtrsim 1$  is due to the role of concentration fluctuations. Even though the fluctuations vanish at late times, they have an irreversible impact on the total reaction.

Under strong segregation, the leading coefficient varies with  $Da$  for two reasons. First, the initial condition to be used with the asymptotic equation differs as above. Second, the weak ergodicity breaking displayed by the inter-reaction times impedes  $\langle C_I(t) C_M(t) \rangle \rightarrow \bar{c}_{0,I} \langle C_M(t) \rangle$  for late times, because there is a sufficiently high probability that  $C_M(t)$  remains large due to long nonreactive regions. Nonetheless, simulations suggest that  $\langle C_I(t) C_M(t) \rangle \propto \bar{c}_I(t) \bar{c}_M(t) \approx c_{0,I} \bar{c}_M(t)$  at late times for all values of  $Da$ , see the right panel of Fig. 4, so that the power-law behavior  $\propto t^{-\beta}$  remains unaffected.

## VI. CONCLUSIONS

The link between first-passage and inter-reaction times connects the kinetics of contact processes to spatial heterogeneity and segregation. We have quantified this link for advective transport under spatial segregation of immobile components and formulated the reaction dynamics in terms of a generalized master equation. The evolution of total mass may be obtained from this description, and mass fluxes and spatial reactant distributions may also be easily computed.

In contrast to the classical picture for well-mixed reactions, the resulting large-scale kinetics cannot be fully quantified in terms of the dynamical equations obtained by averaging over the chemical master equation. This is due to the presence of concentration fluctuations on the order of the average values, which result from a combination of the restart mechanism and memory effects, both caused by segregation. For this reason, closed-form rate laws valid for all times do not exist in general. In the case of strong segregation, characterized by infinite-mean inter-reactive-region distances, memory is long range and induces weak ergodicity breaking across trajectories, a typical feature of anomalous transport [39–44].

Future work will focus on extending this approach to more complex transport processes, including effects such as variable velocity within each trajectory [45,46] and local mixing (e.g., diffusion). Moment closure approximations for the rate equations will also be the subject of further study.

## ACKNOWLEDGMENTS

The authors acknowledge the support of the European Research Council (ERC) through Project No. MHetScale (617511).

## APPENDIX A: WELL-MIXED DEGRADATION KINETICS

Consider the degradation reaction  $\mathcal{S}_M + \mathcal{S}_I \rightarrow_{\kappa} \emptyset$  introduced in the main text. In a well-mixed reactor, the kinetic rate laws are given by Eq. (1). For equal initial conditions,

$\mathbf{c}_0 = (c_{0,M}, c_{0,I})$  with  $c_{0,M} = c_{0,I} = c_0$ , the solution is

$$c_{M,I}^{\text{wm}}(t|\mathbf{c}_0) = \frac{c_0}{1 + \kappa^C c_0 t}. \quad (\text{A1})$$

For  $c_{0,M} \neq c_{0,I}$ , setting  $c_{\max} = \max\{c_M^{\text{wm}}, c_I^{\text{wm}}\}$  and  $c_{\min} = \min\{c_M^{\text{wm}}, c_I^{\text{wm}}\}$ ,

$$\begin{aligned} c_{\min}(t|\mathbf{c}_0) &= c_{0,\min} g(t, \mathbf{c}_0) e^{-\kappa^C t (c_{0,\max} - c_{0,\min})}, \\ c_{\max}(t|\mathbf{c}_0) &= c_{0,\max} g(t, \mathbf{c}_0), \end{aligned} \quad (\text{A2})$$

where

$$g(t, \mathbf{c}_0) = \frac{c_{0,\max} - c_{0,\min}}{c_{0,\max} - c_{0,\min} e^{-\kappa^C t (c_{0,\max} - c_{0,\min})}}. \quad (\text{A3})$$

The simulations of the evolution of concentration due to this reaction in the presence of segregation proceed as follows. A reactive region length  $\ell$  is generated according to the PDF  $\rho_r$ . The solution of the well-mixed rate laws is then applied to obtain the evolution of concentrations for a time interval  $\ell/v$ . Then a nonreactive region length  $\ell'$  is generated according to  $\rho_c$ , and no reaction occurs for a time interval  $\ell'/v$ . This procedure is iterated up to a desired time, with the initial condition for the well-mixed rate laws in each reactive patch being set according to the current mobile concentration and the initial resident immobile concentration.

If one considers instead the catalytic degradation reaction  $\mathcal{S}_M + \mathcal{S}_I \rightarrow_{\kappa} \mathcal{S}_I$  in a well-mixed reactor, then the immobile species concentration does not change and remains equal to  $c_{0,I}$ . The rate law for the mobile component is the same as before, and we obtain

$$c_M^{\text{wm}}(t|\mathbf{c}_0) = e^{-\kappa^C c_{0,I} t}. \quad (\text{A4})$$

The simulations under segregation proceed in the same manner as above, using this solution for the mobile concentration.

## APPENDIX B: INTRINSIC INTER-REACTION TIMES

This Appendix provides a brief review of the intrinsic inter-reaction times, which characterize reactions in the absence of segregation. These correspond to the classical stochastic theory of well-mixed reaction [24]. Consider a given chemical state  $\mathbf{n}$ . Each reaction  $i = 1, \dots, m_r$  considered in isolation has an exponential inter-reaction time with rate  $a_i(\mathbf{n}) = \kappa_i h_i(\mathbf{n})$ , where  $\kappa_i$  is a (microscopic) rate constant and  $h_i(\mathbf{n})$  encodes the dependency on the chemical state. For mass-action reactions,

$$h_i(\mathbf{n}) = \prod_{j=1}^{m_s} \frac{n_j!}{r_{ij}!(n_j - r_{ij})!}. \quad (\text{B1})$$

It follows from the exponential character of reaction times, and the fact that the next reaction to fire is the one with the minimum waiting time, that the inter-reaction time density is

$$\phi_i^r(t|\mathbf{n}) = \frac{a_i(\mathbf{n})}{a(\mathbf{n})} \phi^r(t|\mathbf{n}), \quad (\text{B2})$$

where  $a(\mathbf{n}) = \sum_{i=1}^{m_r} a_i(\mathbf{n})$  and

$$\phi^r(t|\mathbf{n}) = a(\mathbf{n}) e^{-a(\mathbf{n})t}, \quad (\text{B3})$$



with  $\phi'(t|\mathbf{n}) dt$  the probability that the inter-reaction time is in  $[t, t + dt]$ . The Laplace transform of the inter-reaction time density is thus

$$\tilde{\phi}'_i(\lambda|\mathbf{n}) = \frac{a_i(\mathbf{n})}{\lambda + a(\mathbf{n})}. \quad (\text{B4})$$

### APPENDIX C: NUMBER OF TRAVERSED REACTIVE REGIONS

Here we determine the distribution  $v_r(\cdot|t_r, v)$  of the number  $\eta_r(t_r, v)$  of fully traversed reactive regions between reactions, given time  $t_r$  spent in reactive regions and velocity  $v$ . The length traversed in time  $t_r$  is  $vt_r$ . The number  $\eta_r(t_r, v)$  of reactive regions traversed in this time is such that their total length is smaller than  $vt_r$ , but the total length of  $\eta_r(t_r, v) + 1$  regions is larger than  $vt_r$ . Thus,

$$v_r(k|t_r, v) = \left\langle H\left(vt_r - \sum_{k'=1}^k L_{r,k'}\right) H\left(\sum_{k'=1}^{k+1} L_{r,k'} - vt_r\right) \right\rangle, \quad (\text{C1})$$

where  $H$  is the Heaviside step function and the  $L_{r,k'}$  are independent and identically distributed according to  $\rho_r$ . Conditioning on the total length of the first  $k$  regions, we obtain

$$v_r(k|t_r, v) = \int_0^{vt_r} d\ell \left\langle \delta\left(\ell - \sum_{k'=1}^k L_{r,k'}\right) \right\rangle \int_{vt_r-\ell}^{\infty} d\ell' \rho_r(\ell'). \quad (\text{C2})$$

Taking the Laplace transform with respect to  $t_r$ ,

$$\tilde{v}_r(k|\lambda, v) = \frac{1 - \tilde{\psi}_r(\lambda|v)}{\lambda} \tilde{\psi}_r(\lambda|v)^k. \quad (\text{C3})$$

Thus, using  $\rho_r(\ell) = e^{-\ell/\ell_r}/\ell_r$  and  $\psi_r(t|v) = v\rho_r(vt)$ , we have  $\tilde{v}_r(k|\lambda, v) = \mu(v)[1 + \mu(v)\lambda]^{-k}$ , with  $\mu(v) = \ell_r/v$ . Inverting the Laplace transform,

$$v_r(k|t_r, v) = \frac{[t_r/\mu(v)]^k}{k!} e^{-t_r/\mu(v)}, \quad (\text{C4})$$

so that  $\eta_r(t_r, v)$  is Poisson-distributed with mean  $t_r/\mu(v)$ .

Note that, as long as reactive region lengths have a finite mean  $\ell_r$ , we have, for small  $\lambda \ll 1/\mu(v)$  (corresponding to the large  $t_r \gg \mu(v)$  limit),  $\tilde{\psi}_r(\lambda|v) \approx 1 - \mu(v)\lambda \approx 1/[1 + \mu(v)\lambda]$ , the Laplace transform of the exponential density. Thus, the distribution of the number of traversed reactive patches is always approximately Poisson for large  $t_r$ . Since typical reaction times are large when the Damköhler number is low, as explained in the main text, the specific distribution of reactive lengths does not play a role in that case.

### APPENDIX D: GENERALIZED MASTER EQUATION UNDER RESTART

Consider the process  $\mathcal{K}(t)$ , which describes the number of reactions as a function of time, and write  $N_{\mathcal{K}(t)} = \mathbf{N}(t)$ . We have  $\mathcal{K}(t) = \sup\{k | T_k < t\}$ , where  $T_k$  is the time of the  $k$ th reaction. The propagator can then be written as

$p(\mathbf{n}, t|\mathbf{n}_0, v) = \langle \delta_{\mathbf{n}, N_{\mathcal{K}(t)}} | \mathbf{n}_0, v \rangle$ . Conditioning on  $K(t) = k$  and  $T_k = t'$ ,

$$p(\mathbf{n}, t|\mathbf{n}_0, v) = \int_0^\infty dt' \sum_{k \geq 0} \langle \delta_{\mathbf{n}, N_k} \delta(T_k - t') \rangle \times H(t - t') H[\tau_k - (t - t')] | \mathbf{n}_0, v, \quad (\text{D1})$$

with the inter-reaction times  $\tau_k = T_{k+1} - T_k$  independent of  $T_k$ . Thus,

$$p(\mathbf{n}, t|\mathbf{n}_0, v) = \int_0^t dt' \sum_{k \geq 0} R_k(\mathbf{n}, t' | \mathbf{n}_0, v) \times \sum_{i=0}^{m_r} \int_{t-t'}^\infty dt'' \phi_i(t'' | \mathbf{n}, v), \quad (\text{D2})$$

where  $R_k(\mathbf{n}, t|\mathbf{n}_0, v) = \langle \delta_{\mathbf{n}, N_k} \delta(T_k - t) | \mathbf{n}_0, v \rangle$  is the probability per time of arriving at state  $\mathbf{n}$  at time  $t$  given  $k$  reaction steps. The dynamics are Markov in reaction step number  $k$ , and  $R_k(\mathbf{n}, t|\mathbf{n}_0, v)$  solves the Chapman-Kolmogorov equation

$$R_{k+1}(\mathbf{n}, t|\mathbf{n}_0, v) = \int_0^t dt' \sum_{\mathbf{n}' \geq 0} \sum_{i=0}^{m_r} \gamma_i(\mathbf{n}|\mathbf{n}', v) \times \phi_i(t - t' | \mathbf{n}', v) R_k(\mathbf{n}', t'), \quad (\text{D3})$$

with  $R_0(\mathbf{n}, t|\mathbf{n}_0, v) = \delta_{\mathbf{n}, \mathbf{n}_0} \delta(t)$ ,  $\gamma_i(\mathbf{n}|\mathbf{n}', v) = \gamma_i(\mathbf{n}|\mathbf{n}')$  given by Eq. (4), and  $\gamma_0(\mathbf{n}|\mathbf{n}', v)$  given by Eq. (14). Laplace transforming Eqs. (D2) and (D3) summed over  $k$ ,

$$\tilde{R}(\mathbf{n}, \lambda|\mathbf{n}_0, v) = \delta_{\mathbf{n}, \mathbf{n}_0} + \sum_{\mathbf{n}' \geq 0} \sum_{i=0}^{m_r} \gamma_i(\mathbf{n}|\mathbf{n}', v) \times \tilde{\phi}_i(\lambda|\mathbf{n}', v) \tilde{R}(\mathbf{n}', \lambda|\mathbf{n}_0, v),$$

$$\tilde{p}(\mathbf{n}, \lambda|\mathbf{n}_0, v) = \tilde{R}(\mathbf{n}, \lambda|\mathbf{n}_0, v) \frac{1 - \sum_{i=0}^{m_r} \tilde{\phi}_i(\lambda|\mathbf{n}, v)}{\lambda}, \quad (\text{D4})$$

where  $R(\mathbf{n}, t|\mathbf{n}_0, v) = \sum_{k \geq 0} R_k(\mathbf{n}, t|\mathbf{n}_0, v)$ . Eliminating  $\tilde{R}$ , we find

$$\lambda \tilde{p}(\mathbf{n}, \lambda|\mathbf{n}_0, v) - \delta_{\mathbf{n}, \mathbf{n}_0} = \sum_{\mathbf{n}' \geq 0} \sum_{i=0}^{m_r} [\gamma_i(\mathbf{n}|\mathbf{n}', v) - \delta_{\mathbf{n}, \mathbf{n}'}] \times \tilde{M}_i(\lambda|\mathbf{n}', v) \tilde{p}(\mathbf{n}', \lambda|\mathbf{n}_0, v), \quad (\text{D5})$$

where  $\tilde{M}_i(\lambda|\mathbf{n}, v)$  is given according to Eq. (6) for all  $0 \leq i \leq m_r$  and with the sum extending to  $i = 0$ . Laplace inversion leads to the same form as the generalized master equation (5), with the sum extending to  $i = 0$ .

### APPENDIX E: STOCHASTIC SIMULATION ALGORITHMS

We describe a generalized Gillespie algorithm that takes into account restart as described in the main text. Velocity  $v$  is to be sampled from the PDF  $\xi(\cdot)$ . In order to simulate dynamics up to time  $t_m$  (or distance  $\ell_m$ ), the following algorithm

should be repeated for a prescribed number of realizations:

(i) Set time  $t = 0$  (or distance  $\ell = 0$ ). Generate  $\mathbf{n}$  according to the initial state distribution.

(ii) Generate  $\ell_1$  according to  $\rho_r$  and  $\Delta t_r$  according to  $\phi^r(\cdot|\mathbf{n})$ , see Eq. (B3).

(iii) Find the next reaction  $i$ : If  $\Delta t_r > \ell_1/v$ , then set  $i = 0$ . Else generate  $0 < r \leq a(\mathbf{n})$  from the uniform distribution and set  $i$  such that  $a_i(\mathbf{n}) < r \leq a_{i+1}(\mathbf{n})$ , see Eq. (B3).

(iv) If  $i = 0$ , then generate  $\ell_2$  according to  $\rho_c$  and set  $\Delta t = (\ell_1 + \ell_2)/v$ . Else set  $\Delta t = \Delta t_r$ . Increment  $t$  by  $\Delta t$  ( $\ell$  by  $v\Delta t$ ).

(v) If  $t < t_m$  ( $\ell < \ell_m$ ), then update  $\mathbf{n}$  according to  $\gamma_i(\cdot|\mathbf{n}, v)$ , see Eq. (4), and go to 2. Else set  $t = t_m$  ( $\ell = \ell_m$ ) and end.

For large particle numbers, this procedure may be replaced by a more efficient method to find the concentrations:

(i) Set time  $t = 0$  (or distance  $\ell = 0$ ). Generate  $\mathbf{c}$  according to the initial concentration distribution.

(ii) Generate  $\ell_1$  according to  $\rho_r$  and  $\Delta t_r$  according to  $\phi^r(\cdot|\mathbf{n})$ , see Eq. (B3). Set  $\Delta t = \min\{\Delta t_r, t_m - t\}$ .

(iii) Update  $\mathbf{c}$  according to the well-mixed rate equations over the interval  $[t, t + \Delta t]$ . Increment  $t$  by  $\Delta t$  ( $\ell$  by  $v\Delta t$ ). If  $t = t_m$  ( $\ell = \ell_m$ ) end.

(iv) Generate  $\ell_2$  according to  $\rho_c$ . Increment  $t$  by  $\Delta t = \min\{(\ell_1 + \ell_2)/v, t - t_m\}$  ( $\ell$  by  $v\Delta t$ ).

(v) If  $t < t_m$  ( $\ell < \ell_m$ ), then generate  $\mathbf{c}_I$  according to the initial concentration distribution and go to 2. Else end.

Note that this algorithm reduces to the one outlined in Appendix A for the reactions considered therein.

## APPENDIX F: LARGE-SCALE KINETICS

Following Ref. [28], we define  $p^C(\mathbf{c}, t|\mathbf{c}_0, v) = \bar{n}p(\bar{n}\mathbf{c}, t|\bar{n}\mathbf{c}_0, v)$ ,  $M_i^C(t|\mathbf{c}, v) = M_i(t|\bar{n}\mathbf{c}, v)/\bar{n}$ ,  $i = 1, \dots, m_r$ , and  $M_0^C(t|\mathbf{c}, v) = M_0(t|\bar{n}\mathbf{c}, v)$ . We multiply Eq. (D5) by, and sum over,  $\mathbf{n}$ , and write  $\sum_{\mathbf{n}} = \bar{n} \int d\mathbf{c}$  in the limit  $\bar{n} \rightarrow \infty$ . Integrating by parts, we obtain

$$\begin{aligned} & \lambda \tilde{\bar{c}}(\lambda|\mathbf{c}_0, v) - \mathbf{c}_0 \\ &= \sum_{i=1}^{m_r} s_i \mathcal{L}_{t \rightarrow \lambda} \langle \tilde{M}_i^C[\lambda|\mathbf{C}(t)]|\mathbf{c}_0, v \rangle \\ & \quad - \mathcal{L}_{t \rightarrow \lambda} \langle [\mathbf{C}(t) - (\mathbf{C}_M(t), \bar{\mathbf{c}}_{0,I}(v))] \tilde{M}_0^C[\lambda|\mathbf{C}(t)]|\mathbf{c}_0, v \rangle, \end{aligned} \quad (\text{F1})$$

where  $\mathcal{L}_{t \rightarrow \lambda} f(t) = \tilde{f}(\lambda)$ . Substituting Eq. (6) for the memory functions, we have

$$\begin{aligned} & \lambda \tilde{\bar{c}}_M(\lambda|\mathbf{c}_0, v) - \mathbf{c}_{0,M} \\ &= \sum_{i=1}^{m_r} s_i^M \tilde{K}(\lambda|v) \mathcal{L}_{t \rightarrow \lambda} \langle a_i^C[\mathbf{C}(t)]|\mathbf{c}_0, v \rangle, \\ & \lambda \tilde{\bar{c}}_I(\lambda|\mathbf{c}_0, v) - \bar{\mathbf{c}}_{0,I}(v) \left[ 1 + \frac{\tilde{K}(\lambda|v) \tilde{\psi}_c(\lambda|v)}{\mu(v)\lambda} \right] \\ & \quad + \sum_{i=1}^{m_r} s_i^I \tilde{K}(\lambda|v) \mathcal{L}_{t \rightarrow \lambda} \langle a_i^C[\mathbf{C}(t)]|\mathbf{c}_0, v \rangle. \end{aligned} \quad (\text{F2})$$

Using Eq. (3) for the memory kernel, we find that  $1 - \tilde{K}(\lambda|v)[1 - \tilde{\psi}_c(\lambda|v)]/[\mu(v)\lambda] = \tilde{K}(\lambda|v)$ , so that the second equation may be rearranged and divided by  $\tilde{K}(\lambda|v)$  to give

$$\begin{aligned} & \lambda \tilde{\bar{c}}_I(\lambda|\mathbf{c}_0, v) - \bar{\mathbf{c}}_{0,I}(v) = - \frac{\lambda \tilde{\bar{c}}_I(\lambda|\mathbf{c}_0, v) - \bar{\mathbf{c}}_{0,I}(v)}{\mu(v)\lambda} \\ & \quad + \sum_{i=1}^{m_r} s_i^I \mathcal{L}_{t \rightarrow \lambda} \langle a_i^C[\mathbf{C}(t)]|\mathbf{c}_0, v \rangle. \end{aligned} \quad (\text{F3})$$

Inverse-Laplace transforming yields Eq. (17).

In order to integrate Eqs. (17) for the degradation reaction  $\mathcal{S}_M + \mathcal{S}_I \rightarrow \emptyset$ , under the assumption  $\langle C_I C_M \rangle = \bar{c}_I \bar{c}_M$  and mild segregation, note that the memory kernel (3) reads  $\tilde{K}(\lambda|v) = 1 - \alpha/[1 + \alpha + \alpha\mu(v)\lambda]$ , so that, inverting the Laplace transform,  $K(t|v) = \delta(t) - \exp\{-(1 + \alpha)t/[\alpha\mu(v)]\}/\mu(v)$ . Equations (17) then read

$$\begin{aligned} \frac{d\bar{c}_M(t|\mathbf{c}_0, v)}{dt} &= -\kappa^C \bar{c}_M(t|\mathbf{c}_0, v) \bar{c}_I(t|\mathbf{c}_0, v) \\ & \quad + \frac{\kappa^C}{\mu(v)} \int_0^t dt' e^{-\frac{1+\alpha}{\alpha\mu(v)}(t-t')} \bar{c}_M(t'|\mathbf{c}_0, v) \bar{c}_I(t'|\mathbf{c}_0, v), \\ \frac{d\bar{c}_I(t|\mathbf{c}_0, v)}{dt} &= -\kappa^C \bar{c}_M(t|\mathbf{c}_0, v) \bar{c}_I(t|\mathbf{c}_0, v) - \frac{\bar{c}_I(t|\mathbf{c}_0, v) - c_{0,I}}{\mu(v)}. \end{aligned} \quad (\text{F4})$$

We solve these equations numerically using a combination of the forward Euler method for the derivative with the trapezoidal rule for the convolution integral. We use a discretization time step  $\Delta t = 10^{-2} \min\{\mu, 1/(\kappa^C c_{0,M}), 1/(\kappa^C c_{0,I})\}$ .

[1] N. Barkai and S. Leibler, *Nature* **403**, 267 (2000).  
[2] D. Mollison, *J. R. Stat. Soc. B* **39**, 283 (1977).  
[3] R. J. Williams and N. D. Martinez, *Nature* **404**, 180 (2000).  
[4] M. P. Nightingale and C. J. Umrigar, *Quantum Monte Carlo Methods in Physics and Chemistry* (Springer Science & Business Media, New York, 1998).  
[5] C. I. Steefel, D. J. DePaolo, and P. C. Lichtner, *Earth Planet. Sci. Lett.* **240**, 539 (2005).  
[6] D. ben Avraham and S. Havlin, *Diffusion and Reactions in Fractals and Disordered Systems* (Cambridge University Press, Cambridge, 2005).

[7] Y. Meroz, I. M. Sokolov, and J. Klafter, *Phys. Rev. E* **83**, 020104(R) (2011).  
[8] A. M. Tartakovsky, D. M. Tartakovsky, and P. Meakin, *Phys. Rev. Lett.* **101**, 044502 (2008).  
[9] O. Bénichou, C. Chevalier, J. Klafter, B. Meyer, and R. Voituriez, *Nat. Chem.* **2**, 472 (2010).  
[10] A. Godec and R. Metzler, *Phys. Rev. X* **6**, 041037 (2016).  
[11] M. Schmidt, F. Sagués, and I. Sokolov, *J. Phys. Condens. Matter* **19**, 065118 (2007).  
[12] G. J. Lapeyre and M. Dentz, *Phys. Chem. Chem. Phys.* **19**, 18863 (2017).

- [13] A. Ovchinnikov and Y. B. Zeldovich, *Chem. Phys.* **28**, 215 (1978).
- [14] J. M. Sancho, A. Romero, K. Lindenberg, F. Sagués, R. Reigada, and A. Lacasta, *J. Phys. Chem.* **100**, 19066 (1996).
- [15] R. Reigada, F. Sagués, I. M. Sokolov, J. M. Sancho, and A. Blumen, *Phys. Rev. Lett.* **78**, 741 (1997).
- [16] G. Srinivasan, D. M. Tartakovsky, B. A. Robinson, and A. Aceves, *Water Resour. Res.* **43**, W12415 (2007).
- [17] P. C. Lichtner and D. Tartakovsky, *Stoch. Env. Res. Risk. A.* **17**, 419 (2003).
- [18] T. R. Ginn, *Water Resour. Res.* **35**, 1395 (1999).
- [19] P. Grathwohl, H. Rügner, T. Wöhling, K. Osenbrück, M. Schwientek, S. Gayler, U. Wollschläger, B. Selle, M. Pause, J.-O. Delfs *et al.*, *Environ. Earth Sci.* **69**, 317 (2013).
- [20] C. Simmons, T. Ginn, and B. Wood, *Water Resour. Res.* **31**, 2675 (1995).
- [21] T. Ginn, C. Simmons, and B. Wood, *Water Resour. Res.* **31**, 2689 (1995).
- [22] U. Seeboonruang and T. R. Ginn, *J. Contam. Hydrol.* **84**, 127 (2006).
- [23] A. Sanz-Prat, C. Lu, R. T. Amos, M. Finkel, D. W. Blowes, and O. A. Cirpka, *J. Contam. Hydrol.* **192**, 35 (2016).
- [24] D. T. Gillespie, *J. Phys. Chem.* **81**, 2340 (1977).
- [25] D. T. Gillespie, *Physica A (Amsterdam)* **188**, 404 (1992).
- [26] J. L. Doob, *Trans. Am. Math. Soc.* **52**, 37 (1942).
- [27] N. G. van Kampen, *Stochastic Processes in Physics and Chemistry* (Elsevier, Amsterdam, 1992).
- [28] T. Aquino and M. Dentz, *Phys. Rev. Lett.* **119**, 230601 (2017).
- [29] M. J. D. Powell, *Math. Program.* **12**, 241 (1977).
- [30] H. Kautz, E. Horvitz, Y. Ruan, C. Gomes, and B. Selman, *Proc. 18th Nat. Conf. on Artificial Intelligence* Vol. 97 (2002), p. 674.
- [31] S. Reuveni, M. Urbakh, and J. Klafter, *Proc. Natl. Acad. Sci. U.S.A.* **111**, 4391 (2014).
- [32] A. Pal, I. Eliazar, and S. Reuveni, *Phys. Rev. Lett.* **122**, 020602 (2019).
- [33] V. Kenkre, E. Montroll, and M. Shlesinger, *J. Stat. Phys.* **9**, 45 (1973).
- [34] W. Feller, *An Introduction to Probability Theory and Its Applications*, Vol. 2 (John Wiley & Sons, New York, 2008).
- [35] M. M. Meerschaert and A. Sikorskii, *Stochastic Models for Fractional Calculus*, Vol. 43 (Walter de Gruyter, Amsterdam, 2012).
- [36] P. De Anna, T. Le Borgne, M. Dentz, D. Bolster, and P. Davy, *J. Chem. Phys.* **135**, 174104 (2011).
- [37] R. Grima, *J. Chem. Phys.* **136**, 154105 (2012).
- [38] A. Paster, D. Bolster, and D. A. Benson, *J. Comput. Phys.* **263**, 91 (2014).
- [39] R. Klages, G. Radons, and I. M. Sokolov, *Anomalous Transport: Foundations and Applications* (John Wiley & Sons, New York, 2008).
- [40] G. Bel and E. Barkai, *Phys. Rev. Lett.* **94**, 240602 (2005).
- [41] S. Burov, J.-H. Jeon, R. Metzler, and E. Barkai, *Phys. Chem. Chem. Phys.* **13**, 1800 (2011).
- [42] M. A. Lomholt, I. M. Zaid, and R. Metzler, *Phys. Rev. Lett.* **98**, 200603 (2007).
- [43] A. V. Weigel, B. Simon, M. M. Tamkun, and D. Krapf, *Proc. Natl. Acad. Sci. U.S.A.* **108**, 6438 (2011).
- [44] J.-H. Jeon, V. Tejedor, S. Burov, E. Barkai, C. Selhuber-Unkel, K. Berg-Sørensen, L. Oddershede, and R. Metzler, *Phys. Rev. Lett.* **106**, 048103 (2011).
- [45] M. Dentz, P. K. Kang, A. Comolli, T. Le Borgne, and D. R. Lester, *Phys. Rev. Fluids* **1**, 074004 (2016).
- [46] A. Puyguiraud, P. Gouze, and M. Dentz, *Water Resour. Res.* **55**, 1196 (2019).